

# Evaluation of systematic errors on polarization parameters from POLDER instrument data for use in CLARREO Pathfinder-VIIRS intercalibration

Daniel Goldin,<sup>a,b,\*</sup> Rajendra Bhatt<sup>a,b</sup> and Yolanda Shea<sup>b</sup>

<sup>a</sup>ADNET Systems, Inc., Bethesda, Maryland, United States

<sup>b</sup>NASA Langley Research Center, Hampton, Virginia, United States

**ABSTRACT.** One of the Climate Absolute Radiance and Refractivity Observatory Pathfinder (CPF) mission's science objectives is to intercalibrate the reflective solar bands of the NOAA-20 Visible Infrared Imaging Radiometer Suite (VIIRS) instrument against high-accuracy CPF measurements utilizing coincident, co-angled, and co-located footprints acquired over diverse Earth targets. To alleviate the effect of high polarization sensitivity of select VIIRS channels on intercalibration analysis, the CPF team will limit the intercalibration footprints over low-polarized scene types, which will be identified based on an empirical estimation of their degree of polarization (DOP) and angle of polarization (AOP) using Polarization and Directionality of the Earth's Reflectance (POLDER) data. We describe the methodology for evaluating systematic errors in the estimation of DOP and AOP for Earth-reflected radiances using POLDER's polarized bands and investigate their potential impact on CPF-VIIRS intercalibration uncertainty. The systematic errors were found to be  $<0.01$  for DOP and  $<2.2$  deg for AOP, which will have a negligible impact on CPF-VIIRS intercalibration uncertainty.

© The Authors. Published by SPIE under a Creative Commons Attribution 4.0 International License. Distribution or reproduction of this work in whole or in part requires full attribution of the original publication, including its DOI. [DOI: [10.1117/1.JRS.17.034513](https://doi.org/10.1117/1.JRS.17.034513)]

**Keywords:** polarization; systematic; uncertainty; Climate Absolute Radiance and Refractivity Observatory (CLARREO) Pathfinder; CLARREO; Visible Infrared Imaging Radiometer Suite

Paper 230234G received May 25, 2023; revised Sep. 6, 2023; accepted Sep. 12, 2023; published Sep. 26, 2023.

## 1 Introduction

NASA's Climate Absolute Radiance and Refractivity Observatory (CLARREO) Pathfinder (CPF)<sup>1</sup> is an Earth-viewing reflected solar spectrometer that will measure the Earth-reflected solar radiation from the International Space Station with a radiometric uncertainty of 0.3% ( $1\sigma$ ) traceable to the standards of the International System of Units, known as "SI-traceability." The high-accuracy measurements will provide a reference for intercalibrating other in-orbit reflective solar instruments. The spectral range of the CPF instrument is 350 to 2300 nm, with resolution of 6 and 3 nm sampling rate. The CPF's state-of-the-art intercalibration approach will demonstrate the ability to accurately transfer the CPF reference calibration to the shortwave channel (300 to 5000 nm) of the Clouds and the Earth's Radiant Energy System instrument<sup>2</sup> and the reflective solar bands (RSBs) of the Visible Infrared Imaging Radiometer Suite (VIIRS) instrument,<sup>3</sup> both onboard the NOAA-20 spacecraft. The aimed-for intercalibration uncertainty for both target instruments is also 0.3% ( $1\sigma$ ). To satisfy this stringent constraint, the CPF team has developed methods for mitigating the impacts of spatial, spectral,

\*Address all correspondence to Daniel Goldin, [daniel.goldin@nasa.gov](mailto:daniel.goldin@nasa.gov)

polarization, and angular differences between the intercalibration footprints from the CPF and target instruments.

The polarization sensitivity of an instrument may be characterized by evaluating its diattenuation coefficient. The CPF instrument is designed to have low polarization sensitivity, with the diattenuation coefficients  $<0.01$  for wavelengths below 1800 nm and  $<0.02$  above 1800 nm. Of the two intercalibration target instruments, the VIIRS sensor has a significantly higher polarization sensitivity, with diattenuation coefficients up to 0.06 for select shortwave RSBs,<sup>4,5</sup> which has the effect of biasing the intercalibration over highly polarized Earth scenes. To mitigate this impact, the CPF team has developed polarization distribution models (PDMs) to characterize the polarization state in terms of degree of polarization (DOP) and angle of polarization (AOP) of the Earth-reflected radiance as a function of the intercalibration footprint scene type, solar and viewing geometry, and wavelength.<sup>6,7</sup> The PDMs will assist in identifying low-polarized scene radiances by meticulously intercalibrating the polarization-sensitive VIIRS RSBs against the CPF measurements. The empirical PDMs (ePDMs) are derived using the multidirectional Earth-reflected polarized solar radiation measurements from visible and near-infrared channels of the Polarization and Directionality of the Earth's Reflectances (POLDER) instrument<sup>8,9</sup> mounted onboard the Polarization and Anisotropy of Reflectances for Atmospheric Science coupled with Observations from a Lidar (PARASOL) micro-satellite that was operational between 2004 and 2013. The theoretical formulation of the polarization parameters for Earth-reflected radiances using Stokes parameters and their impacts on the at-sensor measurements is discussed below.

A polarization state at the top of the atmosphere (TOA) is specified by three Stokes parameters  $I$ ,  $Q$ , and  $U$ , where  $I$  is radiance, and  $Q$  and  $U$  describe linear polarization. (In the context of most of the TOA remote sensing applications, the fourth Stokes parameter  $V$  is negligibly small and can be ignored.) Alternatively, a polarization state may also be described by the DOP and AOP, expressed in terms of the Stokes components. Throughout the text, we assume Stokes parameters  $Q$ ,  $U$ , and  $I$  to be normalized to the ratio of spectral radiance  $I$  over irradiance at nadir, multiplied by  $\pi$  and are, therefore, taken to be unitless. The DOP, which we will alternately denote as  $P$ , may be expressed in terms of the ratio of the Stokes parameters as

$$P = \frac{\sqrt{Q^2 + U^2}}{I}. \quad (1)$$

From this definition, it follows that the polarization state can range from completely unpolarized ( $Q = 0$  and  $U = 0$ ) to fully polarized ( $I = \sqrt{Q^2 + U^2}$ ).

We denote the angle of linear polarization relative to the scattering plane as  $\psi$ . The light scattered in the atmosphere is predominantly s-polarized, so that  $\psi$  values are found mainly around 90 deg. The angle of linear polarization may also be defined relative to the meridian, or detector, plane and can be expressed in terms of the Stokes parameters as

$$\chi = \frac{1}{2} \arctan(U/Q). \quad (2)$$

The two polarization angles  $\chi$  and  $\psi$  are related as

$$\psi = \chi - \alpha, \quad (3)$$

where  $\alpha$  may be expressed in terms of the three view geometry variables, relative azimuth (RAZ), solar-zenith angle (SZA), and view-zenith angle (VZA) as<sup>10</sup>

$$\tan \alpha = \frac{\sin(\text{SZA})}{\frac{\sin(\text{VZA})}{\tan(\text{SZA})} - \cos(\text{VZA}) \cos(\text{RAZ})}. \quad (4)$$

By default, it is the angle  $\chi$  that is being referred to as the AOP throughout the text. In the forward scattering region, the clear-sky scene types are well-approximated by single scattering with the scattering angle defined here as<sup>11</sup>

$$\cos \Theta = -\cos(\text{VZA}) \cos(\text{SZA}) - \sin(\text{VZA}) \sin(\text{SZA}) \cos(\text{RAZ}). \quad (5)$$

When the light incident upon a detector is polarized and the detector itself is polarization-sensitive, the relationship between the uncorrected and corrected reflectances is given by<sup>5,12</sup>

$$\rho \equiv c_{\rho}\rho_0 = \frac{\rho_0}{1 + aP \cos 2(\chi + \phi)}, \quad (6)$$

where  $\rho_0$  is the uncorrected reflectance and  $\rho$  is the reflectance corrected for detector polarization effects,  $a$  is the detector diattenuation coefficient, and  $\phi$  is the phase shift caused by the detector optics.

The Stokes parameters provided by the POLDER's polarized bands, centered at 490, 670, and 865 nm, are used to construct the ePDMs that quantify the effects of polarization due to scattering in the atmosphere and off Earth's surface. These ePDMs provide DOP and AOP values for CPF-VIIRS intercalibration samples and are categorized based on surface type, atmospheric conditions, and solar and view geometry.<sup>12</sup> Each ePDM is binned in RAZ and VZA and is constrained to a specific SZA range. For every ePDM bin, a mean DOP (or AOP) value is computed from the Stokes parameters. In addition to the means, the corresponding standard deviations are recorded in the same view and solar geometry format as the means. In an idealized ePDM, these standard deviations would be dominated by random uncertainties, also ideally small. This would enable us to improve the intercalibration accuracy by increasing the data sample, as accuracy scales with the square root of the sample size. However, since the ePDMs rely on detector measurements, they are also susceptible to systematic errors. These errors are characterized by a probability distribution whose mean we will refer to as "bias" and its width as the "systematic uncertainty." We will use the term "systematic error" as encompassing both bias and the systematic uncertainty. While measurement bias can often be corrected, systematic uncertainty is irreducible.

Among the many sources of noise in a charge-coupled detector, such as POLDER, there are two dominant sources:<sup>13,14</sup> external photon noise and detector noise. The photon noise is due to fluctuations in the number of photons entering the detector, which may be described by the Poisson distribution (or Gaussian distribution for a large enough statistical sample) whose variance is proportional to radiance. Two sources dominate the detector noise: the dark-current noise in electronics and readout (read) noise, which depends on the frame rate and sampling frequency. In practice, using the data from in-orbit instrument, it is difficult to isolate random photon noise from Rayleigh or Mie scattering in the atmosphere, much less to attribute the type of noise to its source, so from here onward we will use the term "noise" loosely, insofar the empirical observations allow.

Due to the non-negligible polarization sensitivity in some of the VIIRS shortwave channels, as described above, during the initial year of CPF-VIIRS intercalibration, the DOP selection will be constrained to be  $<0.1$ . As we will demonstrate later in this paper, the effect of noise is to bias DOP means toward higher values, with the implication that the  $\text{DOP} < 0.1$  intercalibration sample might be selecting DOP values higher than "true" mean DOP. As CPF strives to achieve the lowest possible intercalibration uncertainty, the focus of this work is to quantify this bias. In addition, a bias in DOP, as well as any potential bias in AOP, will affect the precision of determination of the reflectance [see Eq. (6)].

The effects of noise manifest themselves in terms of uncertainties on Stokes parameters, resulting in systematic effects on DOP and AOP. Although the POLDER team has evaluated the measurement uncertainty in parameter  $U$  in the principal plane,<sup>9</sup> to the best of our knowledge, no direct evaluation of the systematic errors in the DOP and AOP has been performed, which motivated this work. In Secs. 2.1 and 2.2, we will adopt two, in a sense, opposite approaches to determining the noise on DOP and AOP. In determining systematic errors on DOP will try to minimize, as much as possible, the external scattering events in order to isolate the lowest DOP values possible. This will establish the maximum limit on DOP noise, as the lower the DOP values are the higher is the DOP uncertainty,<sup>15,16</sup> with the obvious implication that higher DOP values have lower DOP uncertainty. On the other hand, in determining the systematic errors on AOP, we will make use one of the most highly polarized Earth viewing scenes possible, the clear-sky ocean in the forward scattering region. As the AOP will be shown to be relatively stable across the entire dynamic range of the POLDER measurements, a sharply peaked AOP would allow us to more precisely determine the bias. As the single scattering assumption describes this

type of scene well, a systematic deviation of  $\psi$  from 90 deg is a sign of bias in AOP. In Sec. 3, we use the DOP and AOP biases calculated in Secs. 2.1 and 2.2 to evaluate their impact on the calculated reflectance  $\rho_0$ . Although our study is applicable to the entire polarization domain, we will refer to the CPF-VIIRS DOP < 0.1 regime wherever relevant.

## 2 Determining the DOP Systematic Effects in DOP and AOP

In this study, we consider two types of atmospheric conditions: overcast and clear. We will rely on the former to estimate the bias in the DOP, whereas the latter will be used to evaluate the bias in the determination of the AOP. In both cases, we pick the extremes: to determine the bias in DOP, we will require as unpolarized sample as possible; whereas to determine the bias in AOP, we simply select the most polarized scene type characterized by the POLDER instrument. Unless otherwise indicated, the datasets shown throughout the text represent the entirety of 2006 POLDER data, subject to scene constraints, such as cloud or scene type, but without solar or view geometry restrictions.

### 2.1 Systematic Error in DOP

In order to better understand the influence of the noise on DOP, we illustrate it with the “toy” Monte Carlo simulation. Sets of three random values from three Gaussian distributions represent  $Q$ ,  $U$ , and  $I$  Stokes parameter measurements. The latter have somewhat realistic means (i.e., comparable to POLDER data) but arbitrary standard deviations chosen only to better illustrate the influence of the noise. From each set of random  $Q$ ,  $U$ , and  $I$  values, the corresponding DOP was calculated using Eq. (1). The results are shown in Fig. 1. The same Gaussian means of  $\bar{Q} = 0.01$ ,  $\bar{U} = 0$ , and  $\bar{I} = 0.5$  were used to generate all three DOP distributions; while  $\sigma_Q = 0.02$ ,  $\sigma_U = 0.03$ , and  $\sigma_I = 0.2$  were used to generate Fig. 1(a); for Fig. 1(b),  $\sigma_Q$  and  $\sigma_U$  were increased by a factor of two ( $\sigma_I$  was kept at the same value of 0.2); while for Fig. 1(c),  $\sigma_I$  was increased by a factor of two; while keeping  $\sigma_Q = 0.02$  and  $\sigma_U = 0.03$ , as in Fig. 1(a). The comparison of the plots shows that convolving  $Q$  and  $U$  with additional noise leads to a wider DOP distribution with a higher mean; while adding noise to radiance,

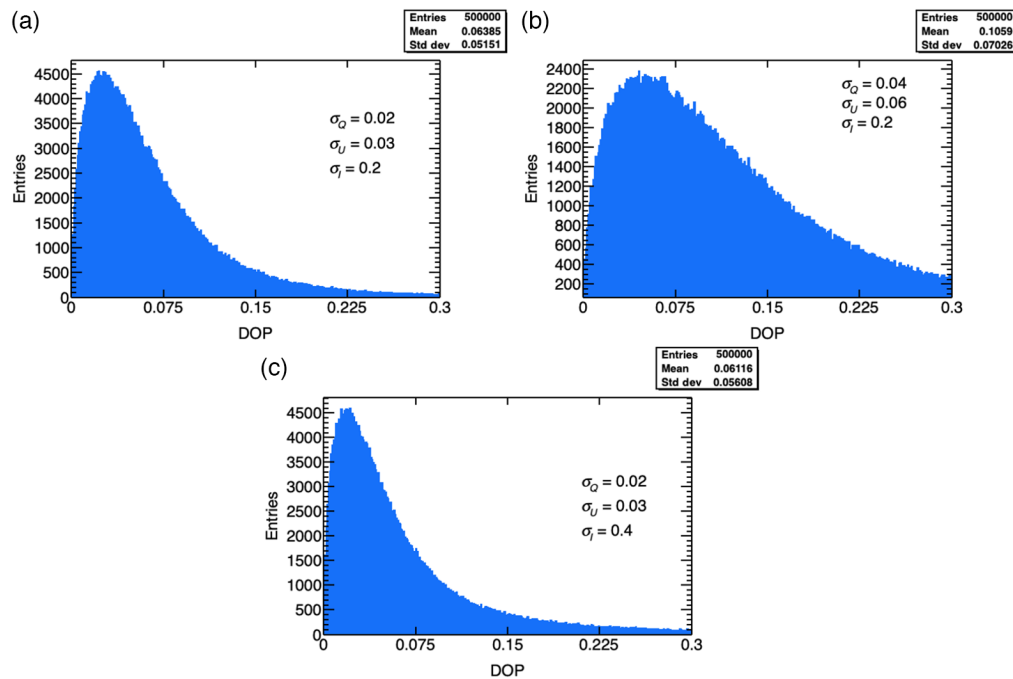


**Fig. 1** Illustration of the influence of noise on the Stokes parameters on DOP. The DOP distributions are computed from the “toy” Monte Carlo-simulated, Gaussian-distributed, normalized Stokes parameters  $Q$ ,  $U$ , and  $I$ . To generate all three DOP distributions, same mean  $Q = 0$ ,  $U = 0$ , and  $I = 0.5$  was used, while the standard deviations were (a)  $\sigma_Q = 0.02$ ,  $\sigma_U = 0.03$ , and  $\sigma_I = 0.2$ ; (b)  $\sigma_Q = 0.04$ ,  $\sigma_U = 0.06$ , and  $\sigma_I = 0.2$ ; and (c)  $\sigma_Q = 0.02$ ,  $\sigma_U = 0.03$ , and  $\sigma_I = 0.4$ .

$I$  has the effect of lowering mean DOP, but, since DOP values are always positive, the overall effect of noise is to always bias DOP toward higher values.

Turning toward the empirically observable polarization, its typical manifestations in the Earth's atmosphere are Rayleigh and Mie scattering, including rainbows, cloudbows, and glories. For clear or partly cloudy conditions, surface reflection and refraction are also significant contributors to polarized light. We would like to identify the as unpolarized sample as possible, with the assumption that the remaining polarization is as close to the combination of photon and detector noise as the measured data allows. This is a conservative approach, since once we are reasonably sure that we have identified the lowest polarized dataset, the systematic uncertainty associated with higher levels of DOP will only be lower.<sup>15,16</sup> Among the observable candidate scene types, we identify snow and ice surfaces, ice clouds, and certain types of water clouds.<sup>9</sup> In terms of polarization characteristics, snow and ice surfaces are similar to ice clouds, but since our goal is to minimize scattering in the atmosphere and due to their relatively low sampling frequency, we disregard the ice- and snow-covered land surfaces.

Of the remaining candidate datasets, in Fig. 2, we compare the DOP as a function of the cloud optical thickness (COT) of (a) ice and (b) water clouds over land for the 865 nm POLDER band. Our studies<sup>17</sup> indicate that for longer wavelengths, such as this one, DOP becomes less sensitive to the chosen land surface type, so a combination of vegetated and non-vegetated surface types is used here. From Fig. 2, two things become apparent: first, the contribution of the surface polarization is overcome by the increased scalar radiance for  $COT > 15$ , where the mean and the standard deviations become nearly invariant. Second, while at some scattering angles ice clouds may be highly polarized, the average DOP is lower for ice clouds than for water clouds. Therefore, as we seek to minimize polarization in the samples used in this analysis, we discard the water cloud dataset and select only the ice clouds for this analysis.

Comparing the zero-slope fits for the DOP versus COT dependence for ice clouds over ocean in Fig. 3 with Fig. 2(a), we note that at sufficiently large values of COT,  $COT > 15$ , the atmospheric contribution dominates the surface contribution.

Finally, to minimize the contribution of the atmospheric scattering, we would like to verify whether the cloud top pressure influences our selection. In Fig. 4, we show how the data sample, which satisfied the previous constraints, is affected by cloud top height. For this selection, we use the ice cloud top pressure measurements performed by the POLDER instrument itself.<sup>18</sup> After the initial plateau, one observes the increase in DOP for pressure higher than 300 hPa, likely due to increased atmospheric scattering lower in the atmosphere. To constrain DOP to the smallest values, the final selection contained data points corresponding to ice cloud top pressure of  $< 300$  hPa.

With the selection of the lowest polarized data sample finalized, we would like to find out in which view geometry the lowest polarization occurs. Parol et al.<sup>19</sup> examined the behavior of polarized reflectance defined as

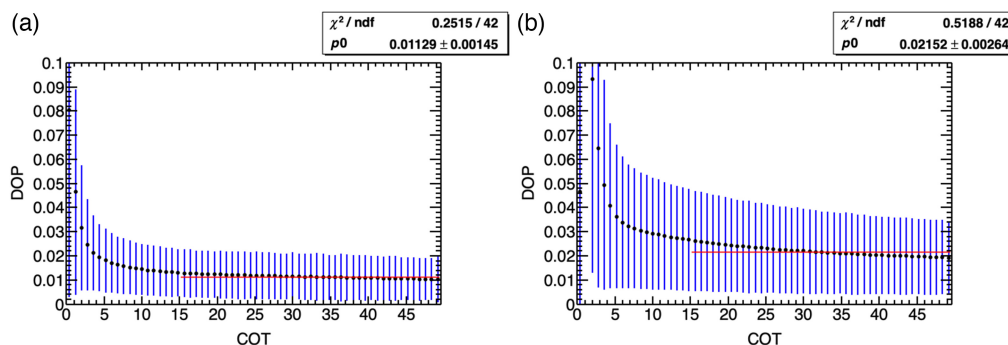


**Fig. 2** DOP versus COT comparison between (a) ice clouds and (b) water clouds over land surfaces for the entirety of POLDER 2006 data. For clarity, DOP bin averages and the corresponding standard deviations are shown in place of scatter plots.  $p_0$  represents the fit parameter for zero-slope fit (solid red line) to the plot for  $COT > 15$ .

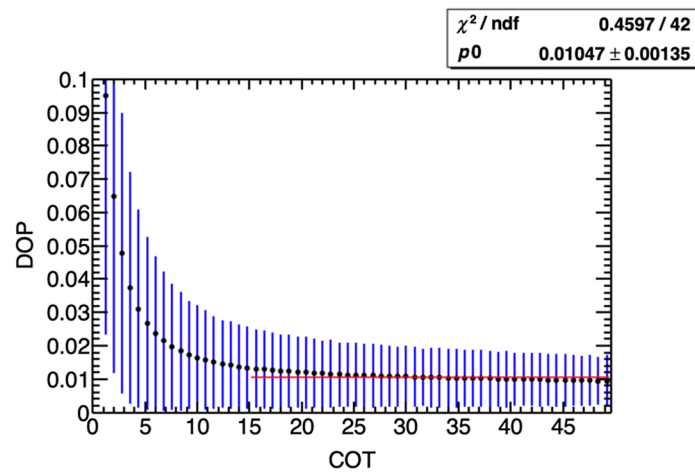


**Fig. 3** DOP versus COT comparison for ice clouds over ocean. For clarity, DOP bin averages and the corresponding standard deviations are shown in place of scatter plots.  $p_0$  represents the fit parameter for zero-slope fit (solid red line) to the plot for COT > 15. This plot is to be compared with ice clouds over land [Fig. 2(a)].

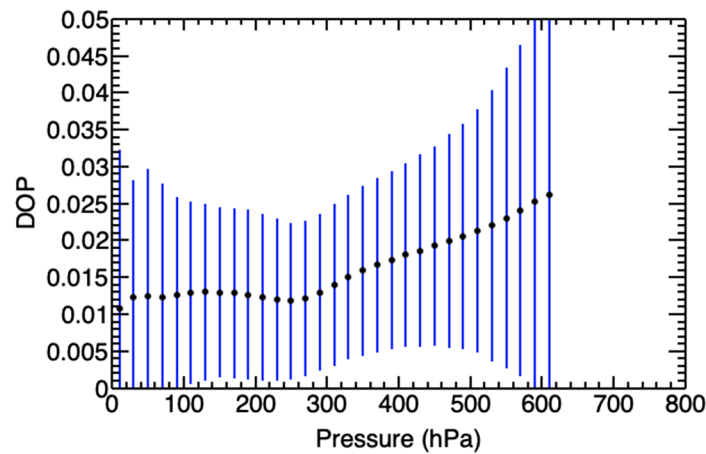


**Fig. 4** DOP versus cloud top pressure dependence for ice cloud scenes. For clarity, DOP bin averages and the corresponding standard deviations are shown in place of scatter plots.

$$\rho_P = \frac{\pi \sqrt{Q^2 + U^2}}{E_s}, \quad (7)$$

where  $E_s$  is the solar irradiance. Based on the simulated polarized reflectance for three different ice crystal shapes and the polarized reflectance measured during 1994 POLDER airborne campaign, the simulated reflectance crosses the point of zero-polarization (with the choice of axes corresponding to  $U = 0$ ) at the scattering angle around 160 deg to 170 deg, known as “neutral point,” while the measured (unsigned) polarized reflectance shows a minimum around the same scattering angle of 170 deg. This conclusion is consistent with our results plotted in Fig. 5 in terms of the DOP versus scattering angle for the 865 nm channel.

The fit around the neutral point in Fig. 5(a) indicates that the DOP bias for the 865 nm is  $\Delta_{P_{865}} = 0.003 \pm 0.001$ , where the uncertainty is the error on the mean. The fact that in our least polarized dataset the neutral point never exactly reaches  $\rho_p = 0$  is an indication of the bias present in DOP determination. In Fig. 5(b), a representative distribution of the standard deviations associated with an ePDM for 865 nm band and  $30 \text{ deg} < \text{SZA} < 40 \text{ deg}$  constraint is shown. Standard deviations of 0.02 and above seem to dominate, with the lowest standard deviations of the order of 0.01 occurring in the backscatter region around  $150 \text{ deg} < \text{VZA} < 180 \text{ deg}$ . Comparing Figs. 5(a) and 5(b), we observe an order of magnitude, or greater, difference between

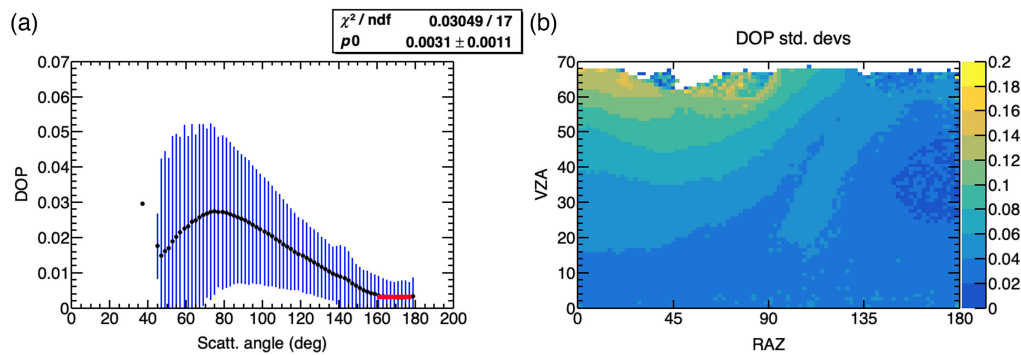


**Fig. 5** (a) DOP versus scattering angle is plotted for the dataset identified by earlier filters (865 nm POLDER band). For clarity, per-bin DOP means and standard deviations are shown in place of a scatter plot. The plateau for scattering angles  $>160$  deg is at the limit of POLDER resolution, as well as an indication of maximum determined bias  $p_0 = 0.0031$  determined from the zero-slope fit (solid red line). (b) For comparison, typical DOP standard deviations associated with the ePDM for  $30 \text{ deg} < \text{SZA} < 40 \text{ deg}$  for the same, 865 nm band. Standard deviations driven by natural variability clearly dominate over the systematic uncertainty in (a).

the typical standard deviations and the systematic error. The same observation holds true for other SZA ranges and rest of the polarized POLDER bands.

Repeating the procedure for the other two POLDER bands, for the 670 nm, the DOP bias was found to be  $0.008 \pm 0.002$ , while for 490 nm the bias is  $0.007 \pm 0.001$ . We note that while these two results are consistent, the DOP bias for the 865 nm channel found earlier appears to be significantly lower than both of those values. Although polarized radiance  $I_p \equiv \sqrt{Q^2 + U^2}$  was determined to be consistent within 10% across all three channels, the 865 nm channel has a bandwidth of 34 nm, which is approximately twice that of the 490 and 670 nm.<sup>9</sup>

## 2.2 Systematic Error in AOP

As mentioned in Sec. 1, AOP in the scattering plane  $\psi$  and the AOP relative to the local (spacecraft) plane of reference AOP ( $\chi$ ) are related and may be expressed solely in terms of view geometry.

In order to determine the systematic error in the AOP, we adopt the approach opposite, in a sense, to how the systematic error in DOP was determined by selecting the most highly polarized scene types available to us, the clear-sky ocean scene. The choice of the clear-sky ocean scene is motivated by the fact that due to the high polarization in the ocean's forward scatter region the mean  $\psi$  may be determined with higher accuracy due to the higher mean and lower standard deviation of its probability density distribution (essentially, higher signal-to-noise ratio) than for other scene types, such as, for example, overcast scenes. The fact that the mean, however, does not vary significantly across the dynamic range is evidenced by  $\psi$  versus radiance plot in Fig. 6. Although the clear-sky ocean scene is used to plot Fig. 6, the other scene types show the same average biased mean across the radiance domain, albeit the accuracy of that mean is lower due to higher uncertainties. To ensure that the highest polarization is selected we constrain the wind speed to be between 2 and 10 m/s and for the 670 and 865 nm channels, where the aerosol optical depth (AOD) was measured, we restrict the AOD to lie between 0 and 0.02. To enhance the single scatter signal, we restrict the view geometry to the forward region, i.e., where the scattering angle  $\Theta < 90$  deg. With the assumption that the uncertainties in view geometry variables are negligible, from Eq. (3), the mean bias in AOP is approximately equal to the bias in  $\psi$ . Using the AOP obtained from POLDER data, we may obtain  $\psi$  for all three POLDER bands. In Fig. 7, we show the  $\psi$  distribution for the 865 nm POLDER band.

From Fig. 7, the bias in  $\psi$  from the 865 nm POLDER band is 2.2 deg. For 490 nm, this bias was found to be 0.5 deg and 2.0 deg for the 670 nm band. Since the AOP  $\chi$ , and, therefore, the variable  $\psi$  is proportional to  $\tan(U/Q)$ , the deviation of  $\psi$  from 90 deg is due to the biased means of the  $Q$  and  $U$  Stokes distributions. This conclusion is confirmed by the relative independence of  $\psi$  on radiance (Fig. 6). Similarly, a “toy” Monte Carlo simulation, analogous to the one in Fig. 1, shows that only varying the means, but not the widths, of  $U$  and  $Q$  distributions can alter

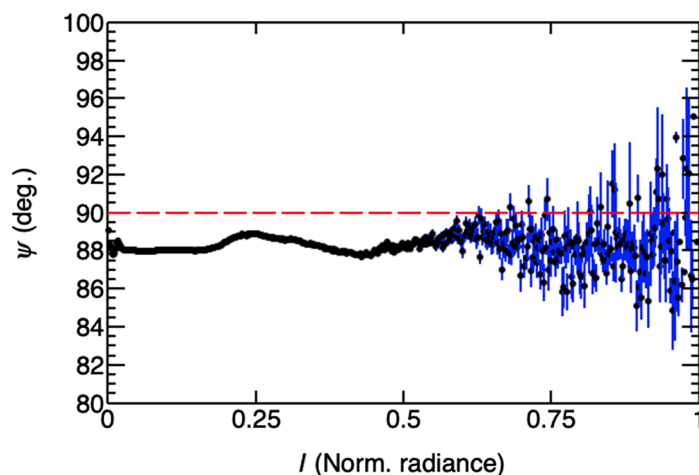


**Fig. 6** Angle  $\psi$  versus normalized radiance shown for the the clear-sky ocean scene at 865 nm, where for clarity, per-bin  $\psi$  means and error of the means (standard errors) are shown in place of a scatter plot. Clear bias away from  $\psi = 90$  deg is seen across the entire dynamic range.

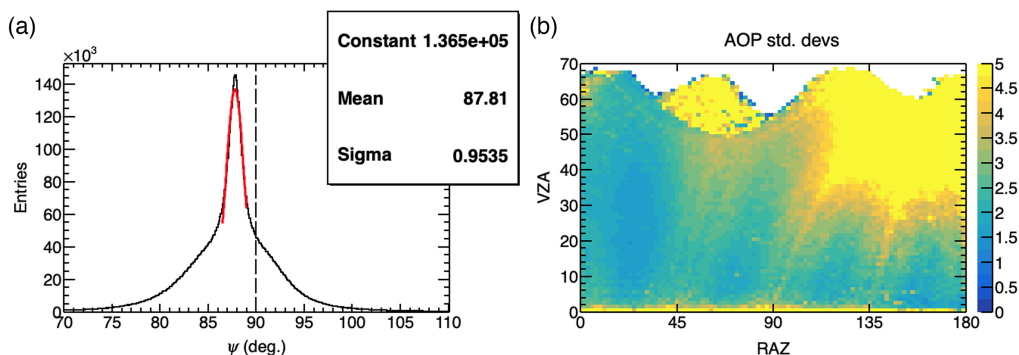


**Fig. 7** (a) Distribution of the  $\psi$  variable defined in Eq. (3) for the 865 nm POLDER band. (b) The 2.2 deg shift obtained from the deviation of the mean of the Gaussian fit (solid red line) from  $\psi = 90$  deg is comparable to the AOP standard deviations for the 865 nm band ePDM (50 deg < SZA < 60 deg). Note that these plots are an AOP analogy to the DOP plots in Fig. 5.

the  $\psi$  mean. The biases are likewise unchanged if we limit the DOP to  $<0.1$ , as we will in the first year of CPF-VIIRS intercalibration. In Fig. 7(b), we show the standard deviations for the ePDM corresponding to the 865 nm band with the 50 deg < SZA < 60 deg constraint. Comparing Figs. 7(a) and (b) reveals that, unlike for the DOP comparison in Fig. 5, the AOP uncertainties (especially in the forward region) are driven to a large extent by the systematic errors. In Sec. 3, we examine the effect the systematic errors have on the uncertainties in the VIIRS/CPF intercalibration. To summarize, the results shown in this section show that the angles of linear polarization derived from data are systematically lower than the “true” values of AOP for all three POLDER bands.

### 3 Effect of Systematic Uncertainties on Intercalibration

A combination of a polarized scene type ( $P > 0$ ) and polarization-sensitive optics causes a bias in the measurement of the radiance or reflectance. This bias would cause the correction factor in Eq. (6) to deviate from unity. We would like to examine the effects of the systematic errors determined in Sec. 2 have on  $c_\rho$ . Although the realistic DOP depends on the scene type and view geometry and the diattenuation coefficient on the detector band and optics configuration, we consider a somewhat artificial scenario, where  $a$  and  $P$  are constant and independent of viewing conditions. We set DOP to  $P = 0.1$ , the threshold value for the first year of the CPF-VIIRS intercalibration, and  $a$  is set to 0.06, which is equal to the largest measured NOAA-20 VIIRS



prelaunch parameter.<sup>5</sup> We take the realistic AOP distribution determined from POLDER data. Under such conditions and assuming optical phase angle of 0, the correction factor, in terms RAZ and VZA, looks like the one shown in Fig. 8. The largest deviations from unity are  $c_\rho = 1.006$  and 0.094.

In principle, one can correct for the bias in the reflectance caused by DOP and AOP biases by shifting both by  $P \rightarrow P - \Delta P$  and  $\chi \rightarrow \chi + \Delta\chi$ . Figure 9 demonstrates the effect of such transformations on the reflectance correction factor  $c_\rho$  (Fig. 8) by plotting the residual differences before and after applying the  $\Delta P = 0.008$  and  $\Delta\chi = \Delta\psi = 2$  deg biases for the 670 nm band from Secs. 2.1 and 2.2).

The residual maxima and minima given for the 670 nm band found in Fig. 9 are  $\pm 6 \times 10^{-4}$ , and they are  $\pm 4 \times 10^{-4}$  and  $\pm 5 \times 10^{-4}$  for the 490 and 865 nm, respectively. We note that only the location in RAZ/VZA space, but not the magnitude, of the maxima and minima of the residuals vary with SZA, so that these maxima and minima are valid across the entire view geometry domain. Comparing these residual differences even with the previous results in Ref. 12 for low-polarized scenes, such as ice clouds, and an order of magnitude lower diattenuation coefficient than used here, we find that for the CPF-VIIRS intercalibration samples with their  $P < 0.1$  requirement, the influence of the systematic errors will be negligibly small.

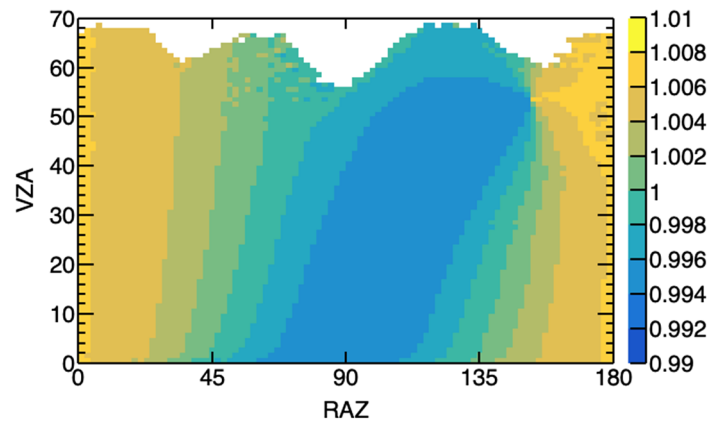


**Fig. 8** Reflectance correction factor  $c_\rho$  for the hypothetical “worst-case” scenario of  $P = 1$  and  $\chi$  calculated from POLDER data. The diattenuation coefficient  $a$  was set to 0.06. For this figure, SZA was restricted to lie between 50 deg and 60 deg.

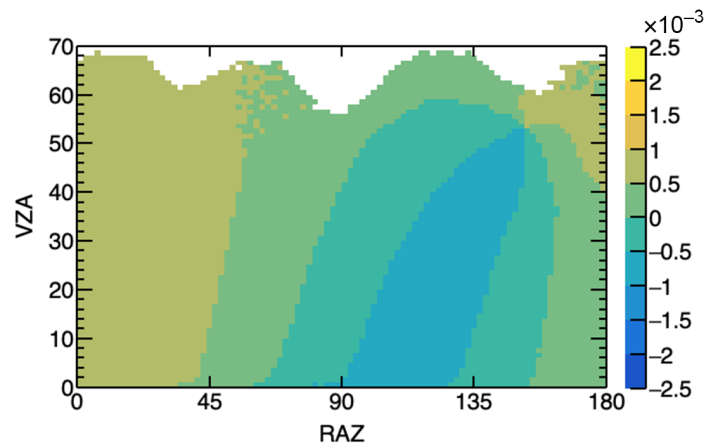


**Fig. 9** Residual differences between  $c_\rho$  (shown in Fig. 8) corrected for systematic bias in two polarization parameters, DOP and AOP, for the 670 nm band and uncorrected  $c_\rho$ .

## 4 Conclusions

The CPF intercalibration team has used POLDER measurements to construct a PDM database to estimate the polarization parameters for the CPF-VIIRS intercalibration samples. As absolutely unbiased measurements are not possible, it is imperative to evaluate the contribution of the systematic errors introduced by the POLDER instrument in the estimation of DOP and AOP, and their potential impact on the intercalibration uncertainty. In this work, we have quantified the expected systematic errors in the DOP and AOP using POLDER's three polarized channels. The systematic errors evaluated here are found to be  $<0.01$  in DOP, which is roughly an order of magnitude smaller than the typical variability of most scene types, and is  $<2.2$  deg in AOP, for all three channels. We also considered how the systematic errors in DOP and AOP may affect the at-sensor reflectance measurements under a somewhat artificial scenario of a completely polarized scene and a polarization-sensitive detector. While, given a highly polarization-sensitive detector channel, as well as certain geometries and highly polarized scene types, a correction due to DOP and AOP bias would make a difference, we found that for most VIIRS bands and our selection of intercalibration samples over low-polarized ( $P < 0.1$ ) Earth scenes and geometry, the effect of these systematic errors on the CPF-VIIRS intercalibration will be negligible.

---

### Data, Materials, and Code Availability

Data used in this work may be found on the POLDER/PARASOL Data and Services on the ICARE website hosted by the University of Lille (France).

### Acknowledgments

The authors would like to thank the anonymous reviewer and François-Marie Bréon of Laboratoire des Sciences du Climat et de l'Environnement (France) for their invaluable critique that has greatly helped to improve this paper. The authors also would like to thank PARASOL data distribution centers at CNES and ICARE, France, for providing access to their data. The authors were supported by CLARREO Pathfinder project funding from the NASA Earth Science Division in the Science Mission Directorate. The authors declare that they have no conflicts of interest.

### References

1. Y. Shea et al., "CLARREO Pathfinder: mission overview and current status," in *IGARSS 2020-2020 IEEE Int. Geosci. and Remote Sens. Symp.*, Waikoloa, Hawaii, pp. 3286–3289 (2020).
2. B. A. Wielicki et al., "Clouds and Earth Radiant Energy System (CERES): an Earth observing system experiment." *Bull. Am. Meteorol. Soc.* **77**, 853–868 (1996).
3. T. E. Lee et al., "The NPOESS VIIRS day/night visible sensor," *Bull. Am. Meteorol. Soc.* **87**, 191–200 (2006).
4. J. Sun et al., "Suomi national polar-orbiting partnership visible infrared imaging radiometer suite polarization sensitivity analysis," *Appl. Opt.* **55**, 7645–7658 (2016).
5. J. Sun et al., "NOAA-20 VIIRS polarization effect and its correction," *Appl. Opt.* **58**, 6655–6665 (2019).
6. C. Lukashin et al., "CLARREO reflected solar spectrometer: restrictions for instrument sensitivity to polarization." *IEEE Trans. Geosci. Remote Sens.* **53**(12), 6703–6709 (2015).
7. D. Goldin and C. Lukashin, "Empirical polarization distribution models for CLARREO-imager intercalibration," *J. Atmos. Ocean. Technol.* **33**, 439–451 (2016).
8. P.-Y. Deschamps et al., "The POLDER mission: instrument characteristics and scientific objectives" *IEEE Trans. Geosci. Remote Sens.* **32**, 598–615 (1994).
9. B. Fougnie et al., "PARASOL in-flight calibration and performance," *Appl. Opt.* **46**, 5435–5451 (2007).
10. F.-M. Bréon, "PARASOL level-1 product data format and user manual; Ed. 1, Rev. 4," PARASOL/ICARE (2016).
11. F. Nadal and F.-M. Bréon, "Parameterization of surface polarized reflectance derived from POLDER spaceborne measurements," *IEEE Trans. Geosci. Remote Sens.* **37**, 1709–1718 (1999).
12. D. Goldin et al., "CLARREO Pathfinder/VIIRS intercalibration: quantifying the polarization effects on reflectance and the intercalibration uncertainty," *Remote Sens.* **11**, 1914 (2019).
13. Y. Zhang et al., "Optimization model of signal-to-noise ratio for a typical polarization multispectral imaging remote sensor" *Sensors* **22**(17), 6624 (2022).
14. G. Kopp et al., "Radiometric flight results from the HyperSpectral Imager for Climate Science (HySICS)," *Geosci. Instrum. Methods Data Syst.* **6**, 169–191 (2017).

15. A. B. Tibbs et al., “Noise creates polarization artefacts,” *Bioinspir. Biomim.* **13**, 015005 (2018).
16. J. F. L. Simmons and B. G. Stewart, “Point and interval estimation of the true unbiased degree of linear polarization in the presence of low signal-to-noise ratios,” *Astron. Astrophys.* **142**, 100–106 (1985).
17. D. Goldin, R. Bhatt, and Y. Shea, “Empirical polarization distribution models for use CLARREO pathfinder-VIIRS intercalibratio,” (manuscript in preparation).
18. P. Goloub et al., “Cloud thermodynamical phase classification from the POLDER spaceborne instrument,” *J. Geophys. Res.: Atmos.* **105**, 14747–14759 (2000).
19. F. Parol et al., “First results of the POLDER Earth Radiation Budget and Clouds operational algorithm,” *IEEE Trans. Geosci. Remote Sens.*, **37**(3), 1597–1612 (1999).

**Daniel Goldin** received his BS degree in physics from the University of California, Santa Cruz, in 1995, his MS degree in physics from the University of California, Davis, in 1997, and his PhD in particle physics from the University of Basel, Switzerland, in 2005. He joined NASA on a contract as a research scientist in 2013. His current research interests are in developing empirical polarization distribution models (ePDMs) and their implementation into the CLARREO Pathfinder (CPF) science framework.

**Rajendra Bhatt** received his MS degree and his PhD in electrical engineering from the South Dakota State University and the University of Virginia, respectively. He is currently supporting the CPF project at NASA Langley Research Center as the deputy project scientist for intercalibration. Prior to joining the CPF team, he worked on the CERES project for 12 years developing techniques for in-flight calibration of geostationary and low Earth-orbiting satellite imagers.

**Yolanda Shea** received her BS degree in Earth and atmospheric science from Cornell University in 2007 and her PhD in atmospheric and oceanic science from the University of Colorado at Boulder in 2012. She has been a research scientist at NASA Langley Research Center since 2012 with a focus on shortwave hyperspectral climate observations and is the project scientist for the CPF mission.